

## Article

# An Advanced Physiological Control Algorithm for Left Ventricular Assist Devices

Mohsen Bakouri <sup>1,2</sup> 

<sup>1</sup> Department of Medical Equipment Technology, College of Applied Medical Science, Majmaah University, Majmaah City 11952, Saudi Arabia; m.bakouri@mu.edu.sa; Tel.: +966-533231905

<sup>2</sup> Department of Physics, College of Arts, Fezzan University, Traghen 71340, Libya

**Abstract:** Left ventricular assist devices (LVADs) technology requires developing and implementing intelligent control systems to optimize pump speed to achieve physiological metabolic demands for heart failure (HF) patients. This work aimed to design an advanced tracking control algorithm to drive an LVAD under different physiological conditions. The pole placement method, in conjunction with the sliding mode control approach (PP-SMC), was utilized to construct the proposed control method. In this design, the method was adopted to use neural networks to eliminate system uncertainties of disturbances. An elastance function was also developed and used as an input signal to mimic the physiological perfusion of HF patients. Two scenarios, ranging from rest to exercise, were introduced to evaluate the proposed technique. This technique used a lumped parameter model of the cardiovascular system (CVS) for this evaluation. The results demonstrated that the designed controller was robustly tracking the input signal in the presence of the system parameter variations of CVS. In both scenarios, the proposed method shows that the controller automatically drives the LVAD with a minimum flow of 1.7 L/min to prevent suction and 5.7 L/min to prevent over-perfusion.

**Keywords:** heart failure; cardiovascular system; left ventricular assist devices; pole placement; sliding mode control; neural network



**Citation:** Bakouri, M. An Advanced Physiological Control Algorithm for Left Ventricular Assist Devices. *Appl. Syst. Innov.* **2023**, *6*, 97. <https://doi.org/10.3390/asi6060097>

Academic Editor: Geng Yang

Received: 4 July 2023

Revised: 21 September 2023

Accepted: 20 October 2023

Published: 24 October 2023



**Copyright:** © 2023 by the author. Licensee MDPI, Basel, Switzerland. This article is an open access article distributed under the terms and conditions of the Creative Commons Attribution (CC BY) license (<https://creativecommons.org/licenses/by/4.0/>).

## 1. Introduction

Heart failure (HF) is a disease that occurs when cardiac muscle exhibits an insufficient capacity to circulate blood adequately [1,2]. A left ventricular assist device (LVAD) has emerged as a valuable solution to help patients suffering from this issue. Different studies have shown that an LVAD positively affects patient outcomes, including increased survival rates, symptom relief, and overall quality of life for individuals with advanced HF [3–5].

LVADs can significantly influence the physiology of the cardiovascular system (CVS) [6,7]. As a result, one of the primary goals of enhancing the state of LVAD technology entails formulating a control approach that can adaptively regulate pump speed to accommodate differences in metabolic requirements [8,9]. Therefore, the physiological control management of this type of device entails monitoring and adjusting device parameters to enhance its efficiency for a given patient. The main goal of LVAD treatment is to provide adequate assistance to the heart and maintain proper blood circulation throughout the body. Therefore, it is necessary to carefully observe the flow rate of the LVAD and determine the volume of blood circulated by the LVAD per unit of time. The LVAD flow rate is tailored to the patient's requirements and can be adjusted up or down to maintain optimal blood pressure and cardiac output. The aspiration inhibition system of LVADs is an essential physiological control parameter. Excessive suction from an LVAD can damage the heart muscle and cause the device to malfunction. The LVADs are equipped with suction prevention mechanisms that supervise intracardiac pressure levels and regulate the device flow rate accordingly to avoid undue suction [10,11].

Various control techniques have been proposed for LVADs, including conventional PID controllers [12,13], optimized controllers [14–16], sliding mode controllers [17,18],

H-infinity controllers based on the estimator model [19], fuzzy logic controllers [20–22], deadbeat controllers [23,24], and predictive model controllers [25–27]. However, these methods may not be effective in dealing with the uncertainty and disturbances common in LVAD systems [28]. Recently, a model-free adaptive control technique has been used to regulate the speed of the LVAD pump in response to changes in the patient's CVS [29]. The methodology in this study designed an algorithm that calculates a coefficient of control over time and then uses existing data on the manipulated and control variables. The performance of this controller was evaluated and verified using computer simulations. The results indicate that LVAD can effectively adapt to changes in blood demand, whether constant or fluctuating. An alternative study presented a supervised adaptive fuzzy control approach featuring pulse-ratio modulation [30]. This study aimed to ensure adequate blood circulation perfusion and reduce the phenomena of aspiration. The results of this study indicate that implementing a supervised adaptive fuzzy controller can effectively prevent the system from experiencing suction hooking compared to conventional approaches. However, most adaptive control techniques suffer from the system convergence phenomenon of chatter, which causes stability convergence to slow down.

Among the above techniques, an extremum-seeking control is a technique that attempts to determine the optimal value of the performance index by processing the control input of the LVAD. Recently, Sadatieh et al. [31] proposed a nonlinear controller that uses an extremum-seeking theory to regulate cardiac performance. The primary objective of the control unit was to improve the pump flow rate while at the same time minimizing the incidence of suction phenomena. An in silico model was used to evaluate the proposed controller, and the results indicate that it can effectively maintain an appropriate cardiac response. Moreover, it is observed that the mean arterial pressure remains within the required range, thus preventing aspiration. The optimization control unit then modulates the LVAD pump speed by analyzing the system's response to the perturbation signal to optimize cardiac output and reduce energy consumption.

Despite an extensive review of LVAD technology, the implementation of physiological control techniques for LVADs is still in its early stages. Further exploration strategies are required for several qualities, including sensorless operation, automated pump speed management, and control reliability. These strategies should be able to drive the LVADs to accurately simulate changes in the patient's preload and CVS adaption [12]. Therefore, the physiological control development of such devices could enhance patients' quality of life with HF and return them to their regular daily routines. To solve the issues related to these control methods, this work proposed the design of a novel control algorithm using the PP-SMC. The technique was developed to minimize tracking errors between the reference and estimated flow while ensuring the system states remain within safe ranges [32]. In this work, the neural network approach drives the system states toward the sliding surface, allowing the SMC technique to achieve quick convergence and robustness against any uncertainties or disturbances. To our knowledge, this is the first study that proposed the use of a PP-SMC neural network method to control an LVAD.

## 2. Materials and Methods

### 2.1. Hemodynamic Characteristics of CVS Model

This work used a software model of the lumped parameters model to examine the proposed control system method [33]. The CVS is combined with the LVAD model in this model, as shown in Figure 1. The hemodynamic characteristics of the CVS system, which contains the right and left side of the heart, regular circulatory system, and pulmonary circulation, are described as

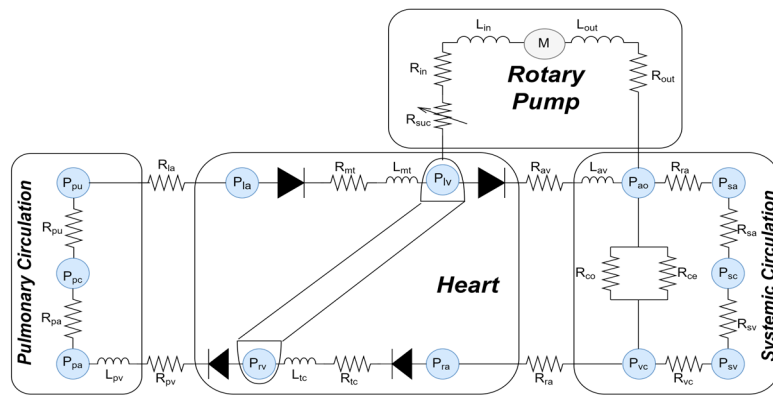


**Figure 1.** The CVS-LVAD rotary pump interaction model.  $R_{in}$ : inlet cannula resistances;  $R_{out}$ : outlet cannula resistances;  $L_{in}$ : inlet cannula inertances;  $L_{out}$ : outlet cannula inertances;  $R_{suc}$ : suction resistance; and  $P_{thor1}$  and  $P_{thor2}$ : intrathoracic pressures.

### 2.1.1. Blood Flow across the Valves

The hemodynamic movement of blood through the cardiac valves (tricuspid, pulmonary, aortic, and mitral valve) is expressed as

$$Q_n = \begin{cases} \frac{p_n - p_{n+1}}{R_n} & p_n \geq p_{n+1} \\ 0 & p_n < p_{n+1} \end{cases} \quad (1)$$

where  $p_n$  is the upstream pressure,  $p_{n+1}$  is the downstream pressure,  $R_n$  represents the resistance of each valve, and  $n$  represents the four cardiac valves.

### 2.1.2. Functions of Blood Vessel in Chambers

The function of blood vessels in chambers for aorta, pulmonary veins, vena cava, and pulmonary peripheral vessel of the CVS are depicted as

$$P_n = \frac{v_n - v_{un,n}}{c_n} \quad (2)$$

where  $v_n$  is the volume in vessel,  $v_{un,n}$  is the unstressed volume of the vessel,  $c_n$  is the compliance, and  $n$  represents vessels in chambers.

### 2.2. Blood Flow between Chambers

The circulation of blood between different chambers can be described as follows:

$$Q_n = \frac{p_n - p_{n+1}}{R_n} \quad (3)$$

The term  $R_n$  denotes the resistance of the respective chamber.

In the CVS model, the steady flow resistance ( $R_{in}$  and  $R_{out}$ ) and serial inductance ( $L_{in}$  and  $L_{out}$ ) are utilized for each inflow and outflow cannula to reduce stress and resistance of flow rate changes. The resistance ( $R_{suc}$ ) has been incorporated prior to the intake cannula to emulate suction events.

### 2.3. LVAD Estimator Model

Our research group has developed and validated a dynamic model for estimating the average pump flow ( $Q_p$ ) of an LVAD [28]. Through this development, two auto-regressive (ARX) models with exogenous input were utilized for system modeling and configuration. Pulse-width modulation (PWM) signal was used as input signal for the first ARX model to estimate the pulsatility index of pump rotational speed ( $PI_\omega$ ). Then, the  $PI_\omega$  was utilized as the input for the subsequent ARX model to estimate  $Q_p$ . A recursive least squares approach

was used to estimate the system parameters. Accordingly, the obtained dynamic estimator model can be expressed as follows:

$$\begin{aligned}\chi(n+1) &= A\chi(n) + \delta A\chi(n) + Bu(n) + \xi(n) \\ Q_p(n) &= C\chi(n)\end{aligned}\quad (4)$$

where " $\chi \in R^n$ " represents the states of the system; " $\delta A$ " is the system parameter variation; " $u = PWM$ " represents the control input; " $\xi$ " is the system disturbance; " $Q_p$ " refers to the system output; and " $A, B$ , and  $C$ " represent matrices of appropriate dimensions.

## 2.4. Control Design

### 2.4.1. Control Strategy

This work aims to design a physiological controller that maintains the optimal functioning of the blood pump flow. To achieve this aim, we need to keep the left atrial pressure within the appropriate physiological range to prevent aspiration or pulmonary congestion. Therefore, to implement this method, we assume:

- The aortic valve is totally closed.
- The elastance function ( $E_t$ ) is used to determine the cardiac output.

This entails the following:

- In each cardiac cycle,  $E_t$  is linearly and exponentially varied during end-systole and end-diastole, respectively.
- If the blood flow exceeds the physiological requirement, it is imperative to adjust the estimated value of  $Q_p$ .
- In order to ensure that the pump flow remains at a constant level, it is necessary to increase the reference flow ( $Q_r$ ) in case it falls below the body's physiological requirements.

This mechanism was achieved through the utilization of the following sinusoidal function:

$$Q_r = a + \beta \sin\left(\frac{2\pi t}{T} + \varphi\right) \quad (5)$$

In this equation,  $a$  and  $\beta$  are fixed values,  $T$  represents the cardiac cycle, and  $\varphi$  denotes the phase shift.

Figure 2 depicts the phase shift between  $Q_r$  and  $E_t$ . In this figure, the value of  $Q_r$  was considered zero during the phase shift; nevertheless, the peak value of  $Q_p$  was observed during the end-systole when  $E_t$  was at its maximum value.

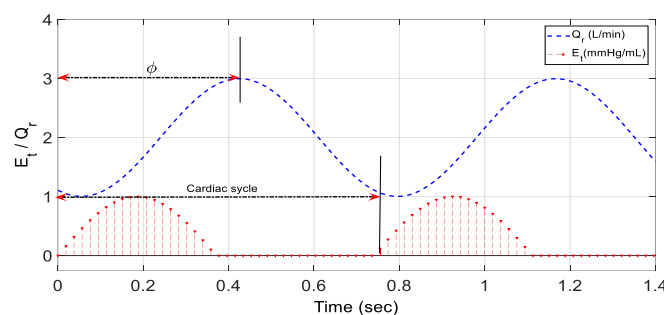


**Figure 2.** Phase shift for  $Q_r$  in comparison with  $E_t$ .

### 2.4.2. Control Algorithm

To implement the control algorithm, we propose to use the pole placement SMC (PP-SMC) approach. In this particular design, the control system matrix is represented by  $(A - BK)$ . The gain matrix ( $K$ ) is derived by assigning n-desired eigenvalues in the pole placement, where  $(K \in R^n)$ . By choosing the suitable  $K$  for state feedback, it is possible to

force the system to have closed-loop poles in the right location where the original system is completely controllable. Therefore, to determine  $K$ , we use Ackermann's formula [34]. Accordingly, the dynamic model in (4) can be written as

$$\begin{aligned}\chi(n+1) &= (A - BK)\chi(n) + \delta A\chi(n) + Bu(n) + \xi(n) \\ Q_p(n) &= C\chi(n)\end{aligned}\quad (6)$$

In this method, we propose using the following sliding surface:

$$\sigma(n) = \gamma e(n) = \gamma(\chi_d(n) - \chi(n)) \quad (7)$$

where  $\gamma$  is the constant vector and formulated to guarantee that the system is asymptotically stable for  $\sigma(n) = 0$ .

From (7), we can write

$$\sigma(n+1) = \gamma e(n+1) = \gamma(\chi_d(n+1) - \chi(n+1)) \quad (8)$$

In order to achieve the requirements of stability and strong reachability, we propose using the Gao formula [35]:

$$\sigma(n+1) = (1 - \Delta T)\sigma(n) - \tau T sign(\sigma(n)) \quad (9)$$

where  $T$  is the sampling period and  $\Delta \geq 0$ ,  $\tau > 0$  satisfies that  $0 < (1 - \Delta T) < 1$ .

Equivalating (6), (8), and (9) gives

$$\begin{aligned}\sigma(n+1) &= \gamma(\chi_d(n+1) - ((A - BK)\chi(n) + \delta A\chi(n) + Bu(n) + \xi(n))) \\ &= (1 - \Delta T)\sigma(n) - \tau T sign(\sigma(n))\end{aligned}\quad (10)$$

Upon solving (10), the control command signal ( $u(n)$ ) is obtained as

$$u(n) = -(\gamma B)^{-1} \begin{pmatrix} \gamma(A - BK)\chi(n) + \gamma\delta A\chi(n) + \gamma\xi(n) - \gamma\chi_d(n+1) \\ + (\Delta T - 1)\gamma\sigma(n) + \tau T sign(\sigma(n)) \end{pmatrix} \quad (11)$$

In this design, Neuro-sliding mode control was employed to eliminate uncertainties and unknown external disturbances. Based on (11), the control command signal ( $u(n)$ ) can be constructed as equivalent neural network ( $u_e(n)$ ) and corrective neural network ( $u_c(n)$ ). Here,  $u_e(n)$  is designed to keep the system states on the  $\sigma(n) = 0$ , while  $u_c(n)$  is trained to force the system states back to  $\sigma(n)$ . Therefore, from (11), we can write

$$u(n) = u_e(n) + u_c(n) \quad (12)$$

For the equivalent part, we can write

$$u_e(n) = -(\gamma B)^{-1}(\gamma((A - BK)\chi(n) + \delta A\chi(n) + \xi(n) - \chi_d(n+1))) \quad (13)$$

For the corrective part, we can write

$$u_c(n) = -(\gamma B)^{-1}(\Delta T - 1)\gamma\sigma(n) + \tau T sign(\sigma(n)) \quad (14)$$

To adjust the values varying the system parameters and disturbances, we propose using neural networks for estimating equivalent, corrective, and control laws. For this reason,  $u_e(n)$  and  $u_c(n)$  are selected to function as a feedforward neural network with three layers, as shown in Figure 3.

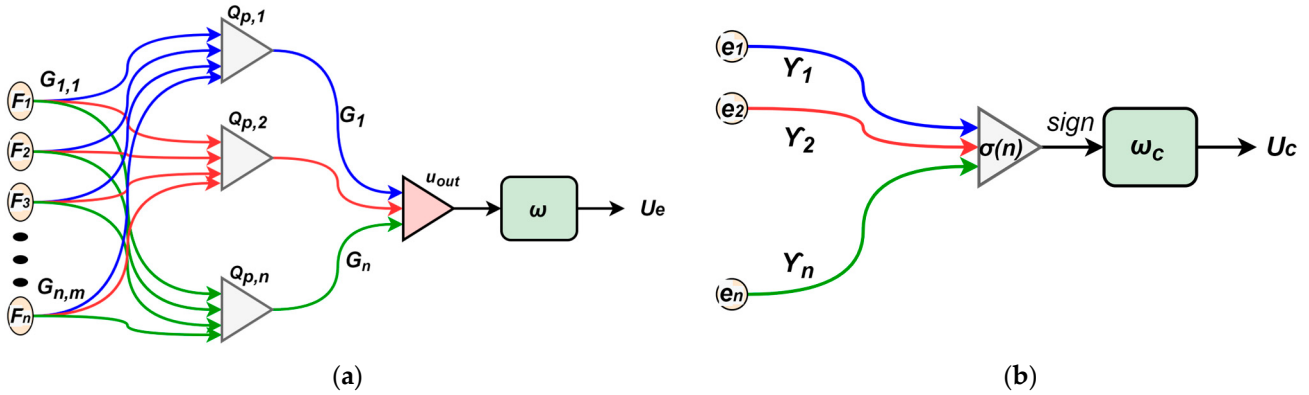


**Figure 3.** Neural networks for estimating control laws; (a) equivalent control; (b) corrective control.

To maintain the system states on the proposed sliding surface ( $\sigma(n) = 0$ ), we need to estimate the equivalent control law as

$$\widehat{u}_e(n) = \omega \cdot \text{sign}(\sigma(n)) \left( \sum_{i=1}^m G_i \cdot \text{sign}(\sigma(n)) \left( \sum_{j=1}^n \bar{G}_{j,i} \cdot F_i \right) \right) \quad (15)$$

In order to restore the plants' state to the sliding surface, we need to train the estimated corrective control law as

$$\widehat{u}_c(n) = \omega_c \cdot \text{sign}(\sigma(n)) \left( \sum_{j=1}^n \gamma_j e_j(n) \right) \quad (16)$$

To achieve a robust estimation for  $\widehat{u}_e(n)$  and  $\widehat{u}_c(n)$ , the training methods employ the following cost functions based on iterative steepest descent algorithm to reduce the mean square errors between the desired and actual values as

$$E = \frac{(u_e(n) - \widehat{u}_e(n))^2}{2} \quad (17)$$

$$T = \frac{(\sigma(n))^2}{2} \quad (18)$$

Based on (17), the weight updating law to reduce (E) can be written as

$$\begin{aligned} \delta G_i &= -\beta \partial E / \partial G_i \\ &= \frac{(\beta \cdot \sigma(n) \cdot \omega \cdot Q_p - \beta \cdot \sigma(n) \cdot \omega \cdot \text{sign}(\sigma(n)) u_{net}^2 Q_p)}{2} \end{aligned} \quad (19)$$

$$\begin{aligned} \delta \bar{G}_{j,i} &= \frac{-\beta \partial E}{\partial \bar{G}_{j,i}} \\ &= \frac{(\beta \cdot \sigma(n) \cdot \omega \cdot G_i - \beta \cdot \sigma(n) \cdot \omega \cdot \text{sign}(\sigma(n)) u_{net}^2 G_i)(1 - \text{sign}(\sigma(n)) Q_p^2)}{4} F_i \end{aligned} \quad (20)$$

where  $\beta > 0$ .

Based on (18), the weight updating law to reduce T can be written as

$$\delta \gamma_j = -\alpha \frac{\partial T}{\partial \gamma_j} = -\alpha \cdot \sigma(n) \cdot e_j(n) \quad (21)$$

where  $\alpha > 0$ .

$K$  in (11) can be calculated based on the updated vector  $\gamma$  as

$$K = \lambda (\gamma^T B)^{-1} \quad (22)$$

where  $\lambda > 0$ . Figure 4 depicts the block diagram of the proposed system.

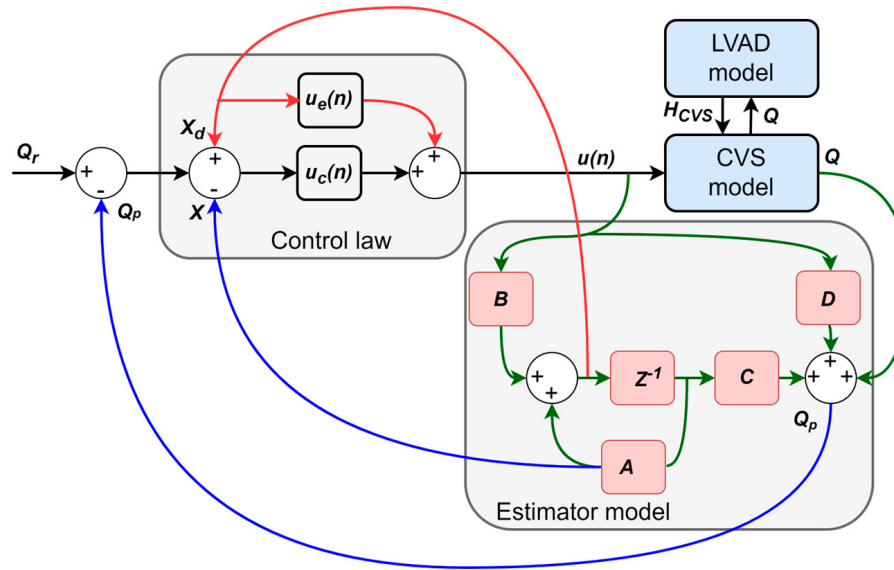


**Figure 4.** Proposed control method. CVS: cardiovascular system; LVAD: Left ventricular assist device;  $H_{cvS}$ : differential pressure;  $Q$ : actual flow;  $Q_p$ : estimated flow;  $Q_r$ : reference flow;  $u_e(n)$ : equivalent control;  $u_c(n)$ : corrective control;  $u(n)$ : control signal.

## 2.5. Software Simulation Environments Protocols

The proposed control method was implemented using MATLAB Simulink “10.5” software tools (The MathWorks Inc., Natick, MA, USA). This method adjusted the CVS model parameters to generate different physiological simulations (rest and exercise) for HF patients. Table 1 illustrates the baseline of the CVS model parameters to represent health and HF conditions. These parameters include the contractility of the left/right ventricle, systemic peripheral resistance, and total blood volume.

**Table 1.** CVS model parameters.

Parameter	HF	Healthy
Systemic peripheral resistance (mm Hg × s/mL)	1.1200	0.7501
Left ventricle contractility (mm Hg/mL)	0.7111	3.4900
Right ventricle contractility (mm Hg/mL)	0.5299	1.7510
Total blood volume (mL)	5798	5298

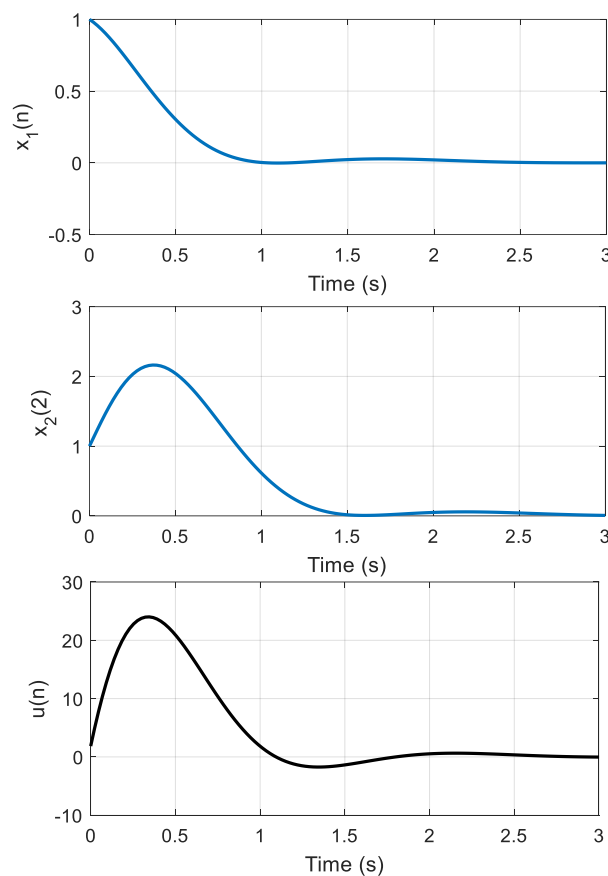
The control method simulated a rest scenario to ensure the controller was robust enough to provide sufficient perfusion support to the HF patient. In this scenario, the CVS model parameters were varied at  $t = 25$  s in one cardiac cycle. This includes decreases in the total blood volume with 500 mL, an increase in the left/right ventricle contractility of 15%, and systemic peripheral resistance kept within the same values.

Subsequently, the simulation was conducted to simulate the transition of system parameters from rest to one physical exertion to ensure that the control algorithm robustly automated the LVAD to provide a minimum flow to the patient. In this scenario, the CVS model parameters were varied at  $t = 25$  s in one cardiac cycle. We keep the system for an additional 35 s in order to give the CVS system enough time to attain a steady state condition. During this scenario, the total blood volume was increased by 500 mL, the left/right ventricle contractility decreased by 20%, and systemic peripheral resistance increased by 15%.

In (10), the parameters for the control law are given as " $\gamma = [1.2 \ -0.95]$ " and " $\tau T = 0.24$ ".

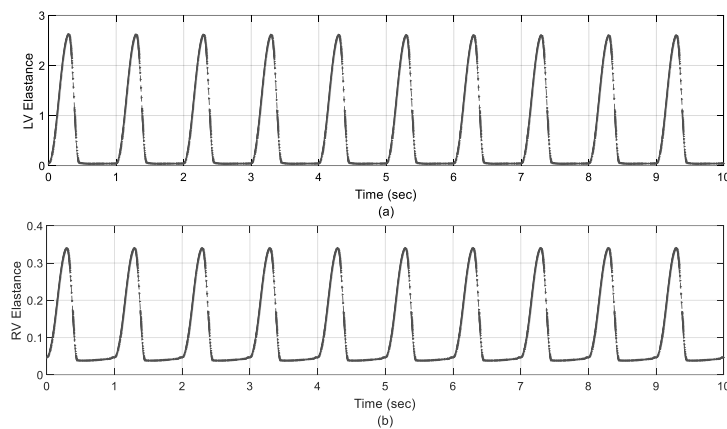
### 3. Results

Figure 5 illustrates the system state responses of the proposed control method using the CVS model. The system stability of the control method was also obtained through the use of the unit step input signal with the initial condition  $[-1 \ 0.5]$ .



**Figure 5.** Responses of system states.

Figure 6 shows the left/right elastance function curves during system simulation, which was designed as the system input signal for CVS. In both scenarios, the results indicate that the controller was able to modulate flexibility to achieve the suggested input signal given in Section 2.4.1. This confirms that the controlled act obtained physiological perfusion to prevent excessive pulmonary aspiration or regurgitation.



**Figure 6.** Left/right elastance of CVS. (a) left elastance function curves during system simulation; (b) right elastance function curves during system simulation.

### 3.1. Results in Rest Scenario

Figure 7 presents the hemodynamic variables of CVS during the rest scenario. The results showed that left ventricular and aortic valve pressure decreased within a safe operating range, as shown in Figure 7a. This means that the control method effectively maintains the systemic flow at a safe operational level by recording 4.5 L/min during this process. As a result, the flow crossing the aortic and mitral valve remained within clinical limits with a maximum recording of 60 mL and 22 mL, respectively, as shown in Figure 7b.

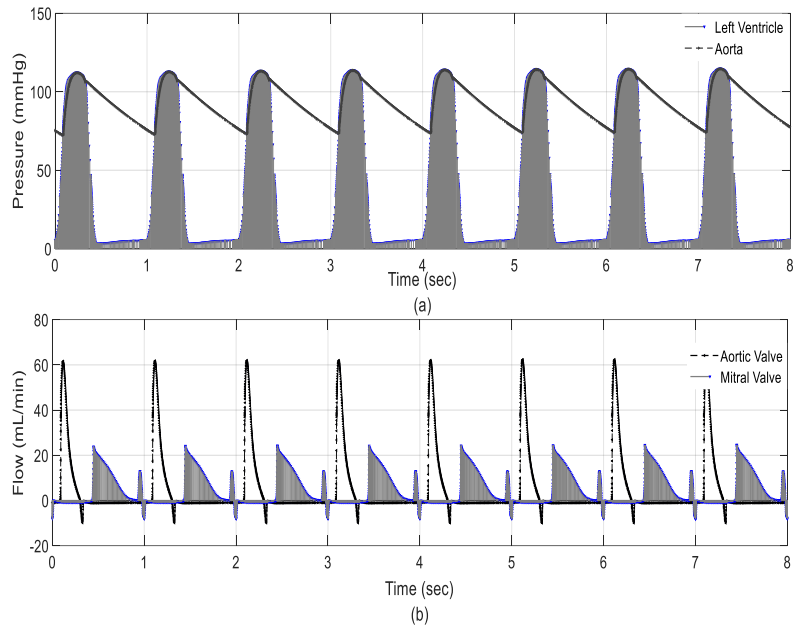


**Figure 7.** Hemodynamic variables. (a): pressure vs. time; (b): flow vs. time.

### 3.2. Results in Exercise Scenario

The results of the hemodynamic variables during the exercise scenario are depicted in Figure 8. The results showed a significant decrease in pressure on the left ventricle and aorta, as shown in Figure 8a. Left ventricular diastolic and systolic pressures decreased to 41 mmHg and 20 mmHg, respectively. Despite these significant reductions, the control algorithm increased the volume of the regular flow by 1.7 L/min to secure the dynamic flow. The results also show that the flow crossing the aortic and mitral valves remained within clinical conditions, as shown in Figure 8b. Table 2 presents hemodynamic variables for CVS in a healthy individual and HF patient.

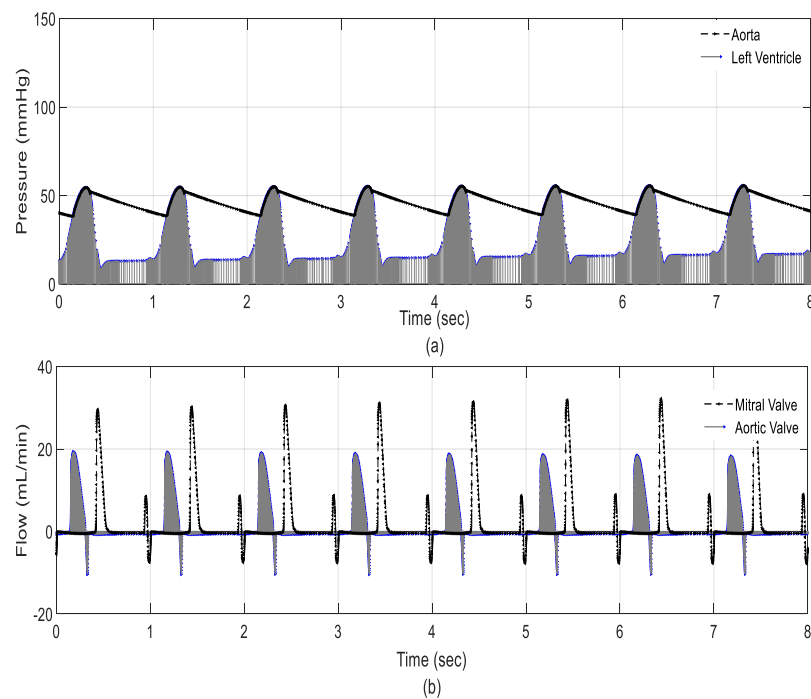


**Figure 8.** Hemodynamic variables. (a): pressure vs. time; (b): flow vs. time.

**Table 2.** CVS variables from the simulation results.

Parameters	Healthy	HF + LVAD	
		Exercise	Rest
Aortic pressure (mmHg)	120	77	105
Left ventricle pressure (mmHg)	120	81	97
Output flow ( $Q_p$ ) (L/min)	5.5	2	2.4

#### 4. Discussion

One of the primary goals needed to improve LVAD technology involves developing a control strategy that automatically adjusts pump speed to meet changes in metabolic demand. In the normal functioning of the heart, the pumping process is subject to the Frank–Starling mechanism [8,9]. This mechanism ensures that the left ventricular stroke volume is adjusted to compensate for left ventricular end-diastolic pressure–volume changes. In order to achieve this theory, in this work, we have chosen the pump flow as a significant parameter for the design of the control system. The elastance function was also chosen as an input signal to acquire a rate of change in the flow that synchronizes the HF patients. The simulation results demonstrated that this function could simulate the proposed flow to balance the physiological status of HF patients, as shown in Figure 5. However, other studies chose the pump differential pressure as an essential control parameter to obtain significant results to simulate HF status [10,12].

In general, LVADs show limited preload sensitivity, indicating their inability to detect or perceive the amount of blood they receive [9]. Thus, it is critical to implement a pump control approach to maintain a safe operating range, where pump flow corresponds to right heart output [36]. Inadequate action may lead to ventricular collapse caused by excessive pumping or decreased preload, reversed pump flow (regurgitation), and pulmonary edema due to insufficient pumping and a consequent decrease in applied differential pressure [37,38]. Therefore, it is essential to approximate direct values of pump flow to obtain the control approach. To achieve this aim, we selected the elastance function as an essential input signal and performed designs so as to obtain a rate of change in the

flow that synchronizes the work of HF patients. The features of this function ensure a minimum average pump flow rate or achieve a maximum differential pressure restriction that requires the careful evaluation of CVS parameters [39].

Eliminating disturbances and parameter variation during controller operation is the significant challenge often found in the operation of this type of pump. Therefore, many control systems are designed to minimize or eliminate these issues [11]. In this regard, this work utilized the neural network method to eliminate any presence of disturbance or parameter variation. This design method introduced the numerical analysis based on PP-SMC while being subject to various physiological situations. According to the findings, the performance of PP-SMC is superior to other control methods [12–27]. For instance, the findings presented in Figures 5–7 and Table 2 demonstrate that the neural PP-SMC can increase tracking performance because it can adaptively alter its parameters based on CVS parameters. Our results also indicate that employing this control strategy will eventually decrease error tracking between the reference and estimated outputs. Due to the reduced elastance on control tracking performance, the estimated pump flow output will follow the reference output flow of 1.5 to 7 L/min. This may cause fewer amplitude oscillations and result in fewer ventricular suctions and pulmonary congestion occurrences. It is evident from the findings that in the two patient scenarios (rest to exercise, reducing postural change), lowering postural instability was more likely to occur in the patient with the increased vascular resistance.

Compared to the other controllers' performance, the PP-SMC controller's control tracking performance can be further improved by optimizing the process of determining the controller's parameters. For instance, a valuable feature of the extremum seeking control is its ability to adapt to changes in the system or the surrounding environment without needing a mathematical representation of the system [40]. This feature makes an LVAD highly compatible with the LVAD, which may be subject to fluctuations in a patient's CVS or medical condition. Despite its potential benefits, monitoring for extremes may be subject to measurement noise and other perturbations. In addition, achieving optimal performance may require fine-tuning the perturbation signal and control parameters. Implementing extreme case control as a control strategy for an LVAD requires detailed design and rigorous testing to ensure its safety and efficacy in clinical settings [41].

In terms of limitations, the baroreflex was not modeled in this particular study, which may have affected both performance and hemodynamics. However, the design method of PP-SMC can appropriately compensate for its effects since any changes caused by the baroreflex can be perceived as a nonlinearity similar to a distinct patient state or scenario, which allows it to work properly. In addition, the Frank–Starling technique for achieving a balance between systemic and pulmonary flows has yet to be incorporated into the methodology that has been developed. Physiological control systems similar to Frank–Starling controllers, which configure the flow rate to be a preload function, have been created and demonstrated to be among the most effective of these systems. However, determining the Frank–Starling process for each patient can be challenging due to their various illnesses.

Further studies could be conducted to evaluate this control method in a pulsatile Mock Circulation Loop system that is capable of reproducing various physiological states (*in vitro* testing).

## 5. Conclusions

This work presents the design and development of an advanced control method for operating an LVAD under different physiological conditions. The proposed method uses PP-SMC combined with a neural network to achieve physiological performance in the presence of variability and perturbations in the system parameters. We have developed an equivalent and corrective law for the neural network to eliminate any discrepancies and disturbances that may occur in any conditions. The cost function is proposed in each control law to achieve robust estimation. Two scenarios (rest and exercise) were proposed

to evaluate the control method using a lumped parameter model of CVS implemented in MATLAB Simulink “10.5” software tools. In both scenarios, the parameters of the CVS model varied in terms of left/right ventricular systole, systemic peripheral resistance, and total blood volume to obtain the physiological conditions of the HF patients. The results show that the proposed method can alter CVS parameters to prevent aspiration or over-perfusion.

**Funding:** This research received no external funding.

**Data Availability Statement:** Not applicable.

**Acknowledgments:** The authors extend their appreciation to the Deanship of Scientific Research—Majmaah University for supporting this research work under project number R-2023-670.

**Conflicts of Interest:** The authors declare no conflict of interest.

## References

1. Edelmann, F.; Knosalla, C.; Mörike, K.; Muth, C.; Prien, P.; Störk, S. Chronic Heart Failure. *Dtsch. Arztebl. Int.* **2018**, *115*, 124–130. [[CrossRef](#)] [[PubMed](#)]
2. Benjamin, E.J.; Blaha, M.J.; Chiuve, S.E.; Cushman, M.; Das, S.R.; Deo, R.; de Ferranti, S.D.; Floyd, J.; Fornage, M.; Gillespie, C.; et al. Heart Disease and Stroke Statistics’2017 Update: A Report from the American Heart Association. *Circulation* **2017**, *135*, e146–e603. [[CrossRef](#)] [[PubMed](#)]
3. Montaldo, A.; Loforte, A.; Musumeci, F.; Krabatsch, T.; Slaughter, M. *Mechanical Circulatory Support in End-Stage Heart Failure*; Springer International Publishing: Cham, Switzerland, 2017. [[CrossRef](#)]
4. Soucy, K.G.; Giridharan, G.A.; Choi, Y.; Sobieski, M.A.; Montreal, G.; Cheng, A.; Schumer, E.; Slaughter, M.S.; Koenig, S.C. Rotary pump speed modulation for generating pulsatile flow and phasic left ventricular volume unloading in a bovine model of chronic ischemic heart failure. *J. Hear. Lung Transplant.* **2015**, *34*, 122–131. [[CrossRef](#)] [[PubMed](#)]
5. Mehra, M.R.; Uriel, N.; Naka, Y.; Cleveland, J.C.; Yuzefpolskaya, M.; Salerno, C.T.; Walsh, M.N.; Milano, C.A.; Patel, C.B.; Hutchins, S.W.; et al. A fully magnetically levitated left ventricular assist device-Final report. *N. Engl. J. Med.* **2019**, *380*, 1618–1627. [[CrossRef](#)]
6. Levine, A.; Gass, A. Third-Generation LVADs: Has Anything Changed? *Cardiol. Rev.* **2019**, *27*, 293–301. [[CrossRef](#)]
7. Hoshi, H.; Shinshi, T.; Takatani, S. Third-generation blood pumps with mechanical noncontact magnetic bearings. *Artif. Organs* **2006**, *30*, 324–338. [[CrossRef](#)] [[PubMed](#)]
8. Stevens, M.C.; Stephens, A.; AlOmari, A.H.H.; Moscato, F. *Physiological Control*; Elsevier Inc.: Amsterdam, The Netherlands, 2018. [[CrossRef](#)]
9. Salamonsen, R.F.; Lim, E.; Gaddum, N.; AlOmari, A.-H.H.; Gregory, S.D.; Stevens, M.; Mason, D.G.; Fraser, J.F.; Timms, D.; Karunanithi, M.K.; et al. Theoretical Foundations of a Starling-Like Controller for Rotary Blood Pumps. *Artif. Organs* **2012**, *36*, 787–796. [[CrossRef](#)]
10. AlOmari, A.-H.H.; Savkin, A.V.; Stevens, M.; Mason, D.G.; Timms, D.L.; Salamonsen, R.F.; Lovell, N.H. Developments in control systems for rotary left ventricular assist devices for heart failure patients: A review. *Physiol. Meas.* **2012**, *34*, R1–R27. [[CrossRef](#)]
11. Bozkurt, S. Physiologic outcome of varying speed rotary blood pump support algorithms: A review study. *Australas. Phys. Eng. Sci. Med.* **2015**, *39*, 13–28. [[CrossRef](#)]
12. Wang, Y.; Koenig, S.C.; Wu, Z.; Slaughter, M.S.; Giridharan, G.A. Sensor-based physiologic control strategy for biventricular support with rotary blood pumps. *ASAIO J.* **2018**, *64*, 338–350. [[CrossRef](#)]
13. Stephens, A.F.; Stevens, M.C.; Gregory, S.D.; Kleinheyer, M.; Salamonsen, R.F. In Vitro Evaluation of an Immediate Response Starling-Like Controller for Dual Rotary Blood Pumps. *Artif. Organs* **2017**, *41*, 911–922. [[CrossRef](#)] [[PubMed](#)]
14. Gwak, K.-W.; Ricci, M.; Snyder, S.; Paden, B.E.; Boston, J.R.; Simaan, M.A.; Antaki, J.F. In vitro evaluation of multiobjective hemodynamic control of a heart-assist pump. *ASAIO J.* **2005**, *51*, 329–335. [[CrossRef](#)] [[PubMed](#)]
15. Ketelhut, M.; Schrödel, F.; Stemmler, S.; Roseveare, J.; Hein, M.; Gesenhues, J.; Albin, T.; Abel, D. Iterative Learning Control of a Left Ventricular Assist Device. *IFAC-PapersOnLine* **2017**, *50*, 6684–6690. [[CrossRef](#)]
16. Wu, Y.; Allaire, P.E.; Tao, G.; Adams, M.; Liu, Y.; Wood, H.; Olsen, D.B. A bridge from short-term to long-term left ventricular assist device-Experimental verification of a physiological controller. *Artif. Organs* **2004**, *28*, 927–932. [[CrossRef](#)]
17. Bakouri, M. Evaluation of an advanced model reference sliding mode control method for cardiac assist device using a numerical model. *IET Syst. Biol.* **2018**, *12*, 68–72. [[CrossRef](#)] [[PubMed](#)]
18. Chang, Y.; Gao, B. A global sliding mode controller design for an intra-aorta pump. *ASAIO J.* **2010**, *56*, 510–516. [[CrossRef](#)] [[PubMed](#)]
19. Bakouri, M.; Alassaf, A.; Alshareef, K.; Abdelsalam, S.; Ismail, H.F.; Ganoun, A.; Alomari, A.H. An Optimal H-Infinity Controller for Left Ventricular Assist Devices Based on a Starling-like Controller: A Simulation Study. *Mathematics* **2022**, *10*, 731. [[CrossRef](#)]
20. Huang, F.; Ruan, X.; Fu, X. Pulse-pressure-enhancing controller for better physiologic perfusion of rotary blood pumps based on speed modulation. *ASAIO J.* **2014**, *60*, 269–279. [[CrossRef](#)]

21. Bakouri, M.; Alassaf, A.; Alshareef, K.; Smida, A.; AlMohimeed, I.; Alqahtani, A.; Aboamer, M.A.; Alharbi, Y. A Feasible Method to Control Left Ventricular Assist Devices for Heart Failure Patients: A Numerical Study. *Mathematics* **2022**, *10*, 2251. [CrossRef]
22. Bakouri, M.; Alassaf, A.; Alshareef, K.; AlMohimeed, I.; Alqahtani, A.; Aboamer, M.A.; Alonazi, K.A.; Alharbi, Y. In Silico Evaluation of a Physiological Controller for a Rotary Blood Pump Based on a Sensorless Estimator. *Appl. Sci.* **2022**, *12*, 11537. [CrossRef]
23. Lim, E.; Alomari, A.-H.H.; Savkin, A.V.; Dokos, S.; Fraser, J.F.; Timms, D.L.; Mason, D.G.; Lovell, N.H. A method for control of an implantable rotary blood pump for heart failure patients using non-invasive measurements. *Artif. Organs* **2011**, *35*, E174–E180. [CrossRef] [PubMed]
24. AlOmari, A.H.; Savkin, A.V.; Ayre, P.J.; Lim, E.; Mason, D.G.; Salamonsen, R.F.; Fraser, J.F.; Lovell, N.H. Non-invasive estimation and control of inlet pressure in an implantable rotary blood pump for heart failure patients. *Physiol. Meas.* **2011**, *32*, 1035–1060. [CrossRef] [PubMed]
25. Koh, V.; Pauls, J.; Wu, E.; Stevens, M.; Ho, Y.; Lovell, N.; Lim, E. A centralized multiobjective model predictive control for a biventricular assist device: An in vitro evaluation. *Biomed. Signal Process. Control* **2020**, *59*, 137–148. [CrossRef]
26. Koh, V.C.; Ho, Y.K.; Stevens, M.C.; Salamonsen, R.F.; Lovell, N.H.; Lim, E. Synergy of first principles modelling with predictive control for a biventricular assist device: In silico evaluation study. In Proceedings of the 2017 39th Annual International Conference of the IEEE Engineering in Medicine and Biology Society (EMBC), Jeju, Republic of Korea, 11–15 July 2017; pp. 1291–1294. [CrossRef]
27. Ng, B.C.; Salamonsen, R.F.; Gregory, S.D.; Stevens, M.C.; Wu, Y.; Mansouri, M.; Lovell, N.H.; Lim, E. Application of multiobjective neural predictive control to biventricular assistance using dual rotary blood pumps. *Biomed. Signal Process. Control* **2018**, *39*, 81–93. [CrossRef]
28. Bakouri, M.A.; Savkin, A.V.; AH, A.H.A. Non-linear modelling and control of left ventricular assist device. *Electron. Lett.* **2015**, *51*, 613–615. [CrossRef]
29. Son, J.; Du, Y. Model-Free Adaptive Control of the Failing Heart Managed by Mechanical Supporting Devices. *IFAC-PapersOnLine* **2022**, *55*, 750–755. [CrossRef]
30. Azizkhani, M.; Chen, Y. Supervised Adaptive Fuzzy Control of LVAD with Pulsatility Ratio Modulation. In Proceedings of the 2022 IEEE 18th International Conference on Automation Science and Engineering (CASE), Mexico City, Mexico, 20–24 August 2022; pp. 2429–2434. [CrossRef]
31. Sadatieh, S.; Dehghani, M.; Mohammadi, M.; Boostani, R. Extremum-seeking control of left ventricular assist device to maximize the cardiac output and prevent suction. *Chaos Solitons Fractals* **2021**, *148*, 111013. [CrossRef]
32. Arndt, A.; Nüsser, P.; Lampe, B. Fully autonomous preload-sensitive control of implantable rotary blood pumps. *Artif. Organs* **2010**, *34*, 726–735. [CrossRef]
33. Lim, E.; Dokos, S.; Salamonsen, R.F.; Rosenfeldt, F.L.; Ayre, P.J.; Lovell, N.H. Numerical Optimization Studies of Cardiovascular-Rotary Blood Pump Interaction. *Artif. Organs* **2012**, *36*, E110–E124. [CrossRef]
34. Chiang, H.-K.; Tsai, J.S.H.; Sun, Y.-Y. Extended Ackermann formula for multivariable control systems. *Int. J. Syst. Sci.* **1990**, *21*, 2113–2127. [CrossRef]
35. Gao, W.; Wang, Y.; Homaifa, A. Discrete-time variable structure control systems. *IEEE Trans. Ind. Electron.* **1995**, *42*, 117–122. [CrossRef]
36. Bakouri, M.A.; Salamonsen, R.F.; Savkin, A.V.; AlOmari, A.-H.H.; Lim, E.; Lovell, N.H. A Sliding Mode-Based Starling-Like Controller for Implantable Rotary Blood Pumps. *Artif. Organs* **2014**, *38*, 587–593. [CrossRef] [PubMed]
37. Cysyk, J.; Newswanger, R.; Popjes, E.; Pae, W.; Jhun, C.-S.; Izer, J.; Weiss, W.; Rosenberg, G. Cannula tip with integrated volume sensor for rotary blood pump control: Early-stage development. *ASAIO J.* **2019**, *65*, 318–323. [CrossRef] [PubMed]
38. Horobin, J.T.; Simmonds, M.J.; Nandakumar, D.; Gregory, S.D.; Tansley, G.; Pauls, J.P.; Girnghuber, A.; Balletti, N.; Fraser, J.F. Speed Modulation of the HeartWare HVAD to Assess In Vitro Hemocompatibility of Pulsatile and Continuous Flow Regimes in a Rotary Blood Pump. *Artif. Organs* **2018**, *42*, 879–890. [CrossRef]
39. Meki, M.H.; Wang, Y.; Sethu, P.; Ghazal, M.; El-Baz, A.; Giridharan, G.A. Sensorless Rotational Speed-Based Control System for Continuous Flow Left Ventricular Assist Devices. *IEEE Trans. Biomed. Eng.* **2020**, *67*, 1050–1060. [CrossRef]
40. Gwak, K.W. Application of extremum seeking control to turbodynamic blood pumps. *ASAIO J.* **2007**, *53*, 403–409. [CrossRef]
41. Arndt, A.; Nüsser, P.; Graichen, K.; Müller, J.; Lampe, B. Physiological control of a rotary blood pump with selectable therapeutic options: Control of pulsatility gradient. *Artif. Organs* **2008**, *32*, 761–771. [CrossRef]

**Disclaimer/Publisher’s Note:** The statements, opinions and data contained in all publications are solely those of the individual author(s) and contributor(s) and not of MDPI and/or the editor(s). MDPI and/or the editor(s) disclaim responsibility for any injury to people or property resulting from any ideas, methods, instructions or products referred to in the content.